Gong, Y., Zhang, B., Zhao, L., Zhang, J., Hu, N., & Zhang, C. (2019). R-curve behaviour of the mixed-mode I/II delamination in carbon/epoxy laminates with unidirectional and multidirectional interfaces. *Composite Structures*, *223*, Article 110949. https://doi.org/10.1016/j.compstruct.2019.110949

R-curve behaviour of the mixed-mode I/II delamination in carbon/epoxy laminates with unidirectional and multidirectional interfaces

Yu Gong[a,b,c,*], Bing Zhang[d], Libin Zhao[e,*], Jianyu Zhang[a,*], Ning Hu[a], Chuanzeng Zhang[f]

[a] College of Aerospace Engineering, Chongqing University, Chongqing 400044, China

[b] Key Laboratory of Fundamental Science for National Defence of Aeronautical Digital Manufacturing Process, Shenyang Aerospace University, Shenyang 110136, China

[c] Chongqing Key Laboratory of Heterogeneous Material Mechanics, Chongqing University, Chongqing 400044, China

[d] Bristol Composites Institute (ACCIS), University of Bristol, Queen's Building, University Walk, Bristol BS8 1TR, UK

[e] School of Astronautics, Beihang University, Beijing 100191, China

[f] Department of Civil Engineering, University of Siegen, Siegen, D-57068, Germany

Abstract: To successfully predict the delamination behaviour of the laminated composite structures with fibre bridging, the *R*-curve has to be studied. This work experimentally investigates the complete *R*-curve behaviour of the unidirectional and multidirectional carbon/epoxy composite laminates. The delamination tests use the double cantilever beam (DCB), mixed-mode bending (MMB) and end-notched flexure (ENF) specimens for mode I, mixed-mode I/II and mode II loading, respectively. The test results show that the interfacial ply and mode mixity (φ-ratio) have significant influences on the initial fracture toughness, steady-state fracture toughness and fibre bridging length. The ratio between the steady-state fracture toughness and its initial value is approximately same for both interfaces, which indicates a similar enhanced effect of the fibre bridging on the fracture toughness. The Benzeggagh-Kenane (*B-K*) criterion is capable of representing the relation between the fracture toughness and the φ-ratio. Based on the DCB and MMB test results, the predicted values of the mode II fracture toughness via the *B-K* criterion are very close to the experimental ones, which illustrates

* Corresponding author.
E-mail address: gongyu@cqu.edu.cn (Y. Gong) ; lbzhao@buaa.edu.cn (L. Zhao); jyzhang@cqu.edu.cn (J. Zhang).

the possibility of determining the mode II fracture toughness without executing the mode II delamination tests. Furthermore, a semi-empirical expression is proposed, which can well predict the mixed-mode I/II delamination behaviour.

***Keywords*:** Carbon fibre; Composite laminates; Delamination; *R*-curve

1 Introduction

Laminated carbon fibre reinforced polymer (CFRP) composites with high stiffness and strength-to-weight ratios have been widely used in a large amount of advanced aerospace structures to achieve the goal of reducing the aircraft weight and increasing the fuel efficiency. Despite their excellent mechanical properties, laminated composite structures are susceptible to the initiation and growth of cracks between the plies, a phenomenon known as the delamination. Various external service loadings, or even manufacturing defects may cause a delamination in a composite laminate structure, which may lead not only to a stiffness loss, but also to a considerable degradation in the strength and the expected service life of the composite structure [1-5]. For damage tolerance designs of composite structures, the fracture toughness of the composite materials must be known in order to predict the delamination growth behaviour and hence the strength of the overall structure [6]. The delamination may occur in three distinct loading modes: mode I (opening), mode II (sliding shear) and mode III (tearing shear). In engineering practice, composite structures are usually affected by the mixed mode I/II delamination, while the mode III effects are negligible. Hence, in recent years, extensive studies have been reported on the mixed mode I/II delamination tests of various composite materials [7-12].

As a mixed-mode I/II delamination propagates along an interfacial ply, unbroken fibres may peel off from the matrix resin and join both crack surfaces in the crack wake, as shown in Fig. 1. The bridging fibres, which interconnect the crack faces, may bear some loads and hence reduce the local stresses at the crack-tip [1]. Thus they contribute to an increase in the mechanical energy required for further delamination propagation. Such a toughening mechanism, resulting in an increasing fracture toughness with the crack growth, has been reported by some experimental works as the *R*-curve

behaviour [6,13-16]. The *R*-curve is determined by three critical parameters: initial fracture toughness, stable steady-state fracture toughness and fibre bridging length. In order to realistically characterise the mixed-mode I/II delamination behaviour, the complete *R*-curve should be obtained.

Less abundant, although of major interest, are the publications which take into account the effect of the fibre bridging and the resulted *R*-curve [17]. The majority of the previous works has been focused on studying the initial or stable steady-state fracture toughness. For example, Benzeggagh and Kenane [12], Ducept et al. [18], Boyina et al. [19] investigated the fracture behaviour of the glass/epoxy composite laminate under mixed-mode loading and the effect of the φ-ratio on the fracture toughness. Kim and Mayer [11], Pereira and Morais [9], Naghipour et al. [20] and Zhao et al. [8] quantitatively or qualitatively investigated the dependence of the mixed-mode I/II delamination fracture toughness on the fibre orientation and stacking sequence of the mid-plane plies. Charalambous et al. [21] and Czabaj and Davidson [10] addressed the effect of the temperature on the fracture toughness of a carbon/epoxy material (IM7/8552) system and woven fabric graphite polyimide composite, respectively. The reported test results showed that the mixed-mode toughness increased at elevated temperature and the toughening mechanisms were dependent on the φ-ratio. LeBlanc and LaPlante [7] made an investigation on the effects of the moisture on the mixed-mode I/II delamination growth in a carbon/epoxy composite and found that an exposure to moisture led to a decrease in the mixed-mode I/II delamination resistance. A considerably improved fracture toughness of the laminated composites was observed through an addition of the nanofillers into matrices [22-24]. Even though a great effort has been made in the past to characterise the mixed-mode I/II delamination resistance of the composite laminates, the complete *R*-curve behaviour under the mixed-mode I/II loading was not fully investigated. Indeed, it is meaningful to obtain the complete *R*-curve, because it is more realistic in practice for determining the likelihood of the delamination propagation.

In addition, most previous studies have been focused on the unidirectional laminates while only

limited *R*-curve data are available for multidirectional laminates, which are usually more preferable than the unidirectional ones in practical engineering applications. Significant differences may exist in the delamination behaviour of the multidirectional and unidirectional laminates [20,25,26]. The complex damage mechanisms, such as the crack migration [27,28] and the intra-ply cracking, will affect the amount of the bridging fibres. And it has been reported that the amount of the bridging fibres significantly depends on the interfacial ply [8]. Usually, more bridging fibres seem to occur in the delamination growth along a multidirectional interface than a unidirectional interface, which results in a much higher fracture toughness in the multidirectional laminates. Thus, interfacial plies play an important role in the delamination propagation behaviour. Based on the above discussions, two basic questions arise here: what is the effect of the interfacial ply on the fibre bridging under the mixed-mode I/II loading, and what is its influence on the *R*-curve behaviour? These questions need to be carefully addressed in order to have a better understanding of the fibre bridging effect on the mixed-mode I/II delamination growth, as well as to improve the design level for the damage tolerant composite structures.

The main purpose of the present study, therefore, is to investigate the complete *R*-curve behaviour of the carbon/epoxy unidirectional and multidirectional laminates, and to reveal the effect of the interfacial ply on the *R*-curve behaviour and the influence of the fibre bridging on the mixed-mode I/II delamination growth. In addition, the predictability of the mode II results obtained by the DCB and MMB tests is also investigated. Finally, a semi-empirical expression is proposed for characterising the mixed-mode I/II delamination behaviour.

2 Material and specimen descriptions

The delamination specimens were manufactured from the T800 carbon-fibre/epoxy material system (Cytec Industries Inc). The lamina elastic properties are: E_{11} = 195 GPa, $E_{22} = E_{33}$ = 8.58 GPa, $v_{12} = v_{13}$ = 0.33, v_{23} = 0.48, $G_{12} = G_{13}$ = 4.57 GPa and G_{23} = 2.9 GPa. The average thickness of each lamina is 0.185mm. In this work, two types of the lay-ups are studied: $0_{12}//0_{12}$ and $(+22.5/-22.5)_6//(+22.5/-$

$22.5)_6$, where the symbol '//' denotes the position of the initial delamination introduced during the fabrication process. The +22.5°/-22.5° interface adopted here can minimise the effect of the unwanted crack migration and matrix damage on the measurement of the fracture toughness. In order to produce the pre-crack, a single Teflon film with a thickness of 25μm was inserted across the width of the panel in the mid-plane of the laminate lay-up. After the curing processing in an autoclave according to the supplier's recommendations, the cured panels were checked for flaws with the ultrasonic C-scanning. Only portions without detected flaws were cut by a diamond saw into individual specimens, which have a width of 25mm, a length of 150mm, and a thickness of 3.12 mm. The specimens with the same configurations were used for the DCB, MMB and ENF tests.

3 Test set-up and procedures for the DCB, MMB and ENF tests

The DCB, MMB and ENF tests, as sketched in Fig. 2, were used for the determination of the mode I, mixed-mode I/II and mode II interlaminar fracture toughness, respectively. Three φ-ratios, defined as the ratio between the mode II strain energy release rate (SERR) and the total SERR, i.e., G_{II}/G_T = 0.25, 0.5, 0.75, have been considered for the MMB case. In order to change the φ-ratio, the lever length c of the MMB loading fixture was adjusted for each φ-ratio whilst keeping the half span-length L constant at 55 mm [7]. The detailed values of the lever length used for the MMB tests are listed in Table 1.

Before the tests, the sides of the specimens were coated with a thin layer of a water-soluble typewriter correction fluid to enable a visual observation of the crack propagation during the tests [29]. A light source was used to enhance the observation of the delamination growth. A travelling microscope with a precision of 0.01 mm was used for identifying the exact location of the crack-tip. The corresponding load and displacement at the loading point were automatically recorded by the self-equipped sensor of the loading machine. The DCB and MMB tests were carried out according to the ASTM standard D5528-13 [30] and ASTM standard D6671/D6671M-13e1 [31], respectively. Both the DCB and the MMB tests were conducted in an MTS 880 servo-hydraulic machine equipped

with a load-cell with a capacity of 1500N. In order to ensure that the displacement loading was effectively applied to the central plane of the cantilever beams, an improved version of the quick-mounted hinge referring to Ref. [32] was adopted in all DCB and MMB tests. In order to ensure a slow delamination growth and maximise the number of the data points, a low displacement-controlled loading rate of 0.1 mm/min was used for all DCB and MMB tests.

For the MMB tests, before mounting the MMB specimen to the testing apparatus, a calibration specimen was required to determine the compliance of the loading system. The calibration specimen was a rectangular bar made from steel with an elastic modulus of 193 GPa and a flexural rigidity of about 90.12 N•m^2 as suggested in the standard test procedure. Similar to the MMB specimen, tabs were applied to one end, then the MMB apparatus was loaded with the calibration specimen and the load-displacement response was recorded. The slope of this calibration load-displacement curve was then measured to calculate the compliance of the MMB testing system, which must be accurately determined for each φ-ratio and lever length. After the system calibration, the MMB tests were carried out by using the MMB apparatus (see Fig. 2).

The scheme of the ENF tests refers to Ref. [33], where the ENF specimen was supported on two parallel rollers. The support span 2L was set as 70 mm and the effective crack length should not be less than 24.5 mm. The displacement was continually applied at the middle span position of the specimen until the delamination grew for about 5 mm. Then the loading was stopped and the support span was increased to 100 mm. The effective delamination length was re-adjusted to be 25 mm. The specimen was loaded continuously again until a noticeable momentary load drop occurred. The displacement loading rate for the ENF tests was set as 1 mm/min.

To check the uniformity of SERR width-wise distribution [34], C-scan detections were done for typical tested specimens. And the C-scan images showed that the difference of crack growth in the both sides and heart of the specimen was small.

4 Calculation of the strain energy release rate

The mode I fracture toughness G_{IC} for the static test could be obtained by using the corrected beam theory [30] as

$$G_{IC} = \frac{3P_{IC}\delta_{IC}}{2b\left(a+|\Delta|\right)}\frac{F}{N'}, \tag{1}$$

where P_{IC} and δ_{IC} are the applied load and displacement, respectively. b is the specimen width, F is a correction factor for considering large displacements, N' a correction factor for considering the load-block effect, which is equal to 1 due to the quick-mounted hinge used in this study. And $|\Delta|$ can be obtained from the intercept of a linear plot of the cube root of the measured compliance values $C^{1/3}$ against the delamination length a.

Considering the weight loading of the lever, the G_I and G_{II} values for the mixed-mode I/II delamination are calculated by the following equations:

$$G_I = \frac{12[P_{I/IIC}(3c-L)+P_g(3c_g-L)]^2}{16b^2h^3L^2E_f}(a+|\Delta|)^2, \tag{2}$$

$$G_{II} = \frac{9[P_{I/IIC}(c+L)+P_g(c_g+L)]^2}{16b^2h^3L^2E_f}(a+0.42|\Delta|)^2, \tag{3}$$

where h is half-thickness of the tested specimen, L is half-span length of the MMB test apparatus, P_g is the weight of the lever and the attached loading apparatus, c_g is the distance from the centre of gravity to the centre of the roller, E_f is the bending modulus of the lay-up of the whole specimen.

The mode II fracture toughness G_{IIC} could be obtained by the following equation:

$$G_{IIC} = \frac{9P_{IIC}\delta_{IIC}a^2}{2b(2L^3+3a^3)}\times 10^3, \tag{4}$$

where P_{IIC} is the critical load, δ_{IIC} is the deflection at the loading point, a is the effective crack length, b is the specimen width, and L is half of the support span.

5 Results and discussions

Two or three specimens were tested for each φ-ratio. The data scatter was small, and the typical load-

displacement curves for the laminates with a 0°/0° interface and a +22.5°/-22.5° interface are shown in Fig. 3. The φ-ratio and the interfacial ply have significant influences on the load-displacement curves. The ultimate load increases with the increase of the mode mixity. In addition, the specimen with a +22.5°/-22.5° interface exhibits a lower structural stiffness, ultimate load and delamination onset displacement than the specimen with a 0°/0° interface. This is resulted from the increasing non-zero plies. There is a clear non-linearity prior to the maximum load being reached. For each mid-plane interface case, the load-displacement curve of the specimens increases linearly until some deviation occurs in the linearity (the point of damage initiation), finally followed by an obvious load drop. With the increase of the mode mixity, the load drop is more sudden, which means that the crack propagation is less steady.

5.1 Experimental fracture toughness

The experimentally measured load, displacement and crack length data are used to construct the *R*-curve, which is the graph of the fracture toughness (G) versus the delamination or crack growth length (Δa). The G-Δa curves for the 0°/0° and +22.5°/-22.5° interfaces are shown in Figs. 4 and 5. An obvious *R*-curve behavior is observed for the G-Δa relation. The facture toughness for both interfaces exhibits the same tendency, which increases with the delamination growth length at the early stage and finally arrives at a steady-state value after a certain delamination growth length. For the MMB tests, the fracture toughness increases very rapidly from a low value until it arrives at a constant after a short delamination growth length. On the other hand, Figs. 4 and 5 also show the effect of the mode mixity on the *R*-curves, which leads to a significant increase in the fracture toughness with the increasing mode II loading. In order to quantitatively characterise the *R*-curve behaviour, the analytical formula [8,15,35] as defined by

$$G_{\mathrm{C}}(\Delta a) = G_{\mathrm{Init}} - 2\left(G_{\mathrm{Prop}} - G_{\mathrm{Init}}\right)\left(\frac{\langle l_{\mathrm{bz}} - \Delta a\rangle}{l_{\mathrm{bz}}} - 1\right) - \left(G_{\mathrm{Prop}} - G_{\mathrm{Init}}\right)\left(\frac{\langle l_{\mathrm{bz}} - \Delta a\rangle}{l_{\mathrm{bz}}} - 1\right)^2 \tag{5}$$

to consider the effect of the fibre bridging is adopted here to fit the experimental data. In Eq. (5), G_{Init}

is the fracture toughness value for the crack initiation, G_{Prop} is the steady-state value of the fracture toughness which is constant or stable with respect to the delamination length, <> is the Macauley operator defined as $< x >= \frac{1}{2}(x + |x|)$. l_{bz} is a fitting parameter and defined as the length of the fibre bridging zone, which is the length between the initial crack length and the crack length correspond to the steady-state value of the fracture toughness.

From the data fitting curves, the detailed values of l_{bz}, G_{Init} and G_{Prop} are obtained and listed in Table 2, where the mode II fracture toughness data obtained from the ENF tests are also given. Only the initial fracture toughness G_{IIC} for the tested specimens can be obtained. They are 2078.8 and 2535.3 J/m^2 for the 0°/0° interface and the +22.5°/-22.5° interface, respectively, which are necessary for checking the capability of the *B-K* criterion for predicting the mode II fracture toughness, as discussed in the following subsection 5.2.

From Table 2, it can be seen that the fibre bridging length under the mixed-mode loading is similar for both interfaces. This is consistent with the reported results in Refs. [6,15,22,23]. However, the bridging length under the mixed-mode loading is much shorter than that under the mode I loading. This means that the introduction of a shear loading has a significant influence on the fibre bridging length and makes it easier to achieve that balance status between the fibre pull-out and the fiber breaking. However, it was observed that the φ-ratio has no effect on the fibre bridging length in the glass/epoxy laminates [6,15,22,23]. The reason for this controversy could be that the effect of φ-ratio on the fibre bridging length is dependent on the material system, stacking sequence, the adjacent fibre orientation, the geometry of the specimen and the loading condition. The ratio of G_{Prop}/G_{Init} is almost the same (around 1.2~1.3) for all test cases of the 0°/0° interface, which indicates that the enhancing effect of the fibre bridging on the fracture toughness is independent on the φ-ratio for the 0°/0° interface. Similarly, the ratio of G_{Prop}/G_{Init} also shows a slight variation with the mode mixity for the +22.5°/-22.5° interface in the mixed-mode regime. The interfacial ply stacking sequence has a negligible influence on the enhancing effect due to the fibre bridging under the mixed-mode loading.

However, the ratio of G_{Prop}/G_{Init} is apparently higher in the mode I delamination for the +22.5°/-22.5° interface. This illustrates that more fibre bridging occurs and the effect of the fibre bridging under the mode I loading is dependent on the interfacial plies.

For certain delamination growth lengths, Fig. 6 gives a presentation of the mode I energy contribution versus the mode II energy component. This representation includes the referred pure modes and the mixed-mode values measured using the MMB tests. An apparent "overshoot" phenomena can be seen in the G_I versus G_{II} plot. The experimental measurements of G_C as a function of the φ-ratio are presented in Fig. 7. The *B-K* criterion [12,36] described by

$$G_C = G_{IC} + \left(G_{IIC} - G_{IC}\right)\left(\varphi\right)^{\eta} \tag{6}$$

which is able to capture the overshoot phenomena and one of the most widely applied criteria for predicting the mixed mode I/II delamination behaviour, is used here to quantitatively characterise the G_C versus φ-ratio data. The *B-K* criterion also has the advantage of having only one fitting parameter η, which makes it less prone to over-fitting [7], and is also recommended by the ASTM standard [31] as the preferred interaction envelope for the mixed-mode I/II delamination [37].

Using a least-square fitting to the initial fracture toughness of the DCB and MMB tests, the values of η for the 0°/0° and +22.5°/-22.5° interfaces are 1.75 and 1.61, respectively. Thus, Eq. (6) can be rewritten as

$$G_C = 338.9 + \left(2262.2 - 338.9\right)\left(\varphi\right)^{1.75}, \tag{7}$$

$$G_C = 339.0 + \left(2765.8 - 339.0\right)\left(\varphi\right)^{1.61}, \tag{8}$$

for the 0°/0° and +22.5°/-22.5° interfaces, respectively. As shown in Fig. 7(a), the *B-K* criterion provides a good fitting to the delamination initiation values for both interfaces, with the R-squared values being higher than 0.99 for both cases. The fitted curves are composed of two essential stages: (a) the first stage with $0\% \leqslant \varphi \leqslant 20\%$, where G_C increases progressively with the φ-ratio; (b) the transition stage with $20\% \leqslant \varphi \leqslant 75\%$, where the curve takes a large radius towards higher values of

the fracture toughness than in the previous stage, which is due to the fact that the mode II loading is becoming more important [12].

Similarly, the same data fitting is conducted for the steady-state fracture toughness in Fig. 7(b). The values of η for the 0°/0° and +22.5°/-22.5° interfaces are 2.12 and 2.05, respectively. Thus, in this case Eq. (6) can be rewritten as

$$G_{\mathrm{C}} = 418.9 + \left(3400.4 - 418.9\right)\left(\varphi\right)^{2.12}, \tag{9}$$

$$G_{\mathrm{C}} = 699.0 + \left(3690.1 - 699.0\right)\left(\varphi\right)^{2.05}. \tag{10}$$

The *B-K* criterion also provides a good fitting to the delamination steady-state values for both interfaces, with the R-squared values being higher than 0.98 for both cases.

5.2 Prediction of the initial and steady-state fracture toughness of the mode II delamination

Due to the formation of a significant fracture process zone in the crack-tip vicinity of the composite materials during the delamination propagation, the experimental measurements of the mode II delamination test data always present some difficulties and scatters [38]. For this reason, an idea is evolved to determine the mode II fracture toughness without carrying out experimental tests. In the present work, the applicability of applying the *B-K* criterion for predicting the mode II fracture toughness is thus checked.

In the subsection 5.1, the values of the fitting parameter η have already been determined by fitting the experimental data from the DCB and MMB tests, thus the mode II fracture toughness can be obtained by the *B-K* criterion. The predicted values of the initial and steady-state fracture toughness for both interfaces are listed in Table 3. Because the experimental steady-state mode II fracture toughness is not available in literature, so the corresponding comparison can unfortunately not be made here. However, acceptable agreements are obtained between the predicted values of the initial mode II fracture toughness and those obtained from the *B-K* criterion. It is, therefore, reasonable to conclude that the *B-K* criterion is applicable to predict the mode II fracture toughness in composite materials.

5.3 A semi-empirical expression for predicting the mixed-mode *R*-curve and its validation

In the subsection 5.1, it was observed that the fibre bridging length is approximately the same for the tested specimens under the mixed-mode I/II loading. This conclusion is also confirmed by other experimental works [6,15,22,23]. In addition, the initial and steady-state mixed-mode fracture toughness values can be well characterised by the *B-K* criterion as discussed before. The criteria for characterizing the initial and steady-state fracture toughness are re-written as following in general forms:

$$G_{\mathrm{Init}} = G_{\mathrm{I}}^{\mathrm{init}} + \left(G_{\mathrm{II}}^{\mathrm{init}} - G_{\mathrm{I}}^{\mathrm{init}}\right)(\varphi)^{\eta_{\mathrm{init}}}, \tag{11}$$

$$G_{\mathrm{Prop}} = G_{\mathrm{I}}^{\mathrm{prop}} + \left(G_{\mathrm{II}}^{\mathrm{prop}} - G_{\mathrm{I}}^{\mathrm{prop}}\right)(\varphi)^{\eta_{\mathrm{prop}}}, \tag{12}$$

where $G_{\mathrm{I}}^{\mathrm{init}}$ and $G_{\mathrm{II}}^{\mathrm{init}}$ are the initial values of the mode I and II fracture toughness, respectively; $G_{\mathrm{I}}^{\mathrm{prop}}$ and $G_{\mathrm{II}}^{\mathrm{prop}}$ are the steady-state values of the mode I and II fracture toughness, respectively; and η_{init} and η_{prop} are the corresponding fitting parameters, which are constants for a fixed interface ply.

Substituting Eqs. (11) and (12) into Eq. (5), a semi-empirical expression as defined by

$$\begin{aligned} G_{\mathrm{C}}(\Delta a) = {} & \left[G_{\mathrm{I}}^{\mathrm{init}} + \left(G_{\mathrm{II}}^{\mathrm{init}} - G_{\mathrm{I}}^{\mathrm{init}}\right)(\varphi)^{\eta_{\mathrm{init}}}\right] - 2\left\{\left[G_{\mathrm{I}}^{\mathrm{prop}} + \left(G_{\mathrm{II}}^{\mathrm{prop}} - G_{\mathrm{I}}^{\mathrm{prop}}\right)(\varphi)^{\eta_{\mathrm{prop}}}\right] - \left[G_{\mathrm{I}}^{\mathrm{init}} + \left(G_{\mathrm{II}}^{\mathrm{init}} - G_{\mathrm{I}}^{\mathrm{init}}\right)(\varphi)^{\eta_{\mathrm{init}}}\right]\right\}\left(\frac{\langle l_{\mathrm{bz}} - \Delta a\rangle}{l_{\mathrm{bz}}} - 1\right) \\ & - \left\{\left[G_{\mathrm{I}}^{\mathrm{prop}} + \left(G_{\mathrm{II}}^{\mathrm{prop}} - G_{\mathrm{I}}^{\mathrm{prop}}\right)(\varphi)^{\eta_{\mathrm{prop}}}\right] - \left[G_{\mathrm{I}}^{\mathrm{init}} + \left(G_{\mathrm{II}}^{\mathrm{init}} - G_{\mathrm{I}}^{\mathrm{init}}\right)(\varphi)^{\eta_{\mathrm{init}}}\right]\right\}\left(\frac{\langle l_{\mathrm{bz}} - \Delta a\rangle}{l_{\mathrm{bz}}} - 1\right)^2 \end{aligned} \tag{13}$$

can be obtained for characterizing the mixed-mode I/II *R*-curve behaviour. To verify whether the proposed expression of Eq. (13) can well describe all measured data, this semi-empirical expression is used to predict the mixed-mode I/II *R*-curve behaviour of composite laminates, as the first attempt to demonstrate its accuracy and reliability. Fig. 8 presents a comparison between the experimentally measured and the predicted *G*-Δ*a* curves. The predicted results for the 0°/0° interface at $\varphi = 0.25$ are slightly underestimated. Overall, the predicted results by Eq. (13) are close to the experimental values of the mixed-mode I/II tests, which illustrates the applicability of the proposed semi-empirical expression for predicting the mixed-mode *R*-curve behaviour when the φ-ratio is between 0.25 and 0.75. Although only a limited number of specimens were tested in the present work, it would be

interesting to verify the validity of the semi-empirical expression for composites with several other different fibers and matrixes and interface plies. In addition, *R*-curve relative to the crack growth length is adopted in this study to describe the effect of fiber bridging on delamination behaviour. While the cracking opening displacement can be an alternative parameter more relevant for fibre bridging phenomena and *R*-curve, and related studies on this should also be interesting.

6 Conclusions

In this work, the mixed-mode I/II *R*-curves of the unidirectional and multidirectional laminates made from carbon/epoxy composites were experimentally determined using the mixed-mode bending tests. Additional experiments were conducted to characterise the mode I and mode II delamination behaviour by using the DCB and ENF tests, respectively.

The obtained *R*-curves resulting from the fibre bridging are qualitatively analysed by three critical parameters in terms of the initial and steady-state fracture toughness and the fibre bridging length. It was found that the initial and steady-state fracture toughness values are strongly influenced by the interfacial ply and the φ-ratio. For each considered interface, the fibre bridging length under the mode I loading is much higher than that under the mixed-mode loading. This conclusion is different from the reported results in other references. The interfacial ply has an effect on the fibre bridging length. However, the fibre bridging length in the mixed-mode I/II delamination is approximately the same for each considered interface. The ratio $G_{\mathrm{Prop}}/G_{\mathrm{Init}}$ is almost the same (around 1.2~1.3) for the mixed-mode I/II delamination. It illustrates that the interfacial ply and the φ-ratio do not affect the enhanced effect of the fibre bridging on the fracture toughness in the mixed-mode I/II delamination. Although only two kinds of the interface ply were tested in the present work, the influences of the interfacial ply on the fibre bridging and the resulting *R*-curve behaviour have been investigated at least in a qualitative manner, which may be further confirmed by more experimental data.

The *B*-*K* criterion was used to represent the mixed-mode I/II delamination fracture toughness results, and it was found that it can represent the experimental data with a reasonable accuracy. The

unique parameter in the *B*-*K* criterion can be determined by the curve-fitting techniques after the DCB and MMB tests at limited φ-ratios, such as 0.25, 0.5 and 0.75. By using the obtained *B*-*K* criterion, the mode II fracture toughness can be predicted with a good estimation. Therefore, it provides a simple determination method for the mode II fracture toughness without executing the mode II test. Finally, a semi-empirical expression is proposed to characterise the complete *R*-curve behaviour in the mixed-mode I/II delamination. The predicted results by this semi-empirical expression are close to the test values, which illustrates the applicability of the proposed semi-empirical expression.

Acknowledgements

The research work is supported by the National Natural Science Foundation of China (Project nos. 11872131, 11772028, 11372020 and 11572058), the Chongqing Natural Science Foundation (Project no. cstc2018jcyjAX0235), the Fundamental Research Funds for the Central Universities and the Key Laboratory of Fundamental Science for National Defence of Aeronautical Digital Manufacturing Process of Shenyang Aerospace University (Project no. SHSYS2018001). Yu Gong also gratefully acknowledges the financial support from the German Academic Exchange Service (DAAD) to support his fellowship research at the Chair of Structural Mechanics, University of Siegen, Germany.

References

[1] NS Choi, AJ Kinloch, JG Williams. Delamination fracture of multidirectional carbon-fiber/epoxy composites under mode I, mode II and mixed-mode I/II loading. J Compos Mater 1999; 33: 73-100.
[2] Y Gong, L Zhao, J Zhang, N Hu. A novel model for determining the fatigue delamination resistance in composite laminates from a viewpoint of energy. Compos Sci Technol 2018; 167: 489-96.
[3] L Zhao, Y Wang, J Zhang, Y Gong, Z Lu, N Hu, J Xu. An interface-dependent model of plateau fracture toughness in multidirectional CFRP laminates under mode I loading. Composites Part B: Engineering 2017; 131: 196-208.
[4] Y Wang, X Chen, Y Gong. Experimental Study on Delamination of Composite Laminates with 0°/45° Interface under Mode I, Mode II and Mixed-mode I/II Loading. Journal of Aeronautical Materials 2018; 38: 83-8.
[5] W Li, W Huang, Y Kang, Y Gong, Y Ying, J Yu, J Zheng, L Qiao, S Che. Fabrication and investigations of G-POSS/cyanate ester resin composites reinforced by silane-treated silica fibers. Compos Sci Technol 2019; 173: 7-14.
[6] F Dharmawan, G Simpson, I Herszberg, S John. Mixed mode fracture toughness of GFRP composites. Compos Struct 2006; 75: 328-38.
[7] LR LeBlanc, G LaPlante. Experimental investigation and finite element modeling of mixed-mode delamination in a moisture-exposed carbon/epoxy composite. Compos A Appl Sci Manuf 2016; 81:

202-13.
[8] L Zhao, Y Gong, J Zhang, Y Chen, B Fei. Simulation of delamination growth in multidirectional laminates under mode I and mixed mode I/II loadings using cohesive elements. Compos Struct 2014; 116: 509-22.
[9] AB Pereira, AB de Morais. Mixed mode I+ II interlaminar fracture of glass/epoxy multidirectional laminates-Part 2: Experiments. Compos Sci Technol 2006; 66: 1896-902.
[10] MW Czabaj, BD Davidson. Determination of the mode I, mode II, and mixed-mode I – II delamination toughness of a graphite/polyimide composite at room and elevated temperatures. J Compos Mater 2015; 0: 1-19.
[11] BW Kim, AH Mayer. Influence of fiber direction and mixed-mode ratio on delamination fracture toughness of carbon/epoxy laminates. Compos Sci Technol 2003; 63: 695-713.
[12] ML Benzeggagh, M Kenane. Measurement of mixed-mode delamination fracture toughness of unidirectional glass/epoxy composites with mixed-mode bending apparatus. Compos Sci Technol 1996; 56: 439-49.
[13] Y Gong, L Zhao, J Zhang, Y Wang, N Hu. Delamination propagation criterion including the effect of fiber bridging for mixed-mode I/II delamination in CFRP multidirectional laminates. Compos Sci Technol 2017; 151: 302-9.
[14] Y Gong, L Zhao, J Zhang, N Hu. An improved power law criterion for the delamination propagation with the effect of large-scale fiber bridging in composite multidirectional laminates. Compos Struct 2018; 184: 961-8.
[15] MM Shokrieh, M Heidari-Rarani, MR Ayatollahi. Delamination R-curve as a material property of unidirectional glass/epoxy composites. Mater Design 2012; 34: 211-8.
[16] A Yan, E Marechal, H Nguyen-Dang. A finite-element model of mixed-mode delamination in laminated composites with an R-curve effect. Compos Sci Technol 2001; 61: 1413-27.
[17] P Coronado, A Argüelles, J Viña, J Bonhomme, V Mollón. Influence on the delamination phenomenon of matrix type and thermal variations in unidirectional carbon-fiber epoxy composites. Polym Composite 2014.
[18] F Ducept, D Gamby, P Davies. A mixed-mode failure criterion derived from tests on symmetric and asymmetric specimens. Compos Sci Technol 1999; 59: 609-19.
[19] D Boyina, A Banerjee, R Velmurugan. Mixed-mode translaminar fracture of plain-weave composites. Compos Part B Eng 2014; 60: 21-8.
[20] P Naghipour, M Bartsch, L Chernova, J Hausmann, H Voggenreiter. Effect of fiber angle orientation and stacking sequence on mixed mode fracture toughness of carbon fiber reinforced plastics: Numerical and experimental investigations. Mater Sci Eng: A 2010; 527: 509-17.
[21] G Charalambous, G Allegri, SR Hallett. Temperature effects on mixed mode I/II delamination under quasi-static and fatigue loading of a carbon/epoxy composite. Compos A Appl Sci Manuf 2015; 77: 75-86.
[22] F Ghadami, MR Dadfar, AS Zeraati. Mixed mode I/II delamination analysis of rubber-modified glass-reinforced epoxy composites. J Reinf Plast Comp 2014; 33: 1634-43.
[23] MM Shokrieh, A Zeinedini, SM Ghoreishi. On the mixed mode I/II delamination R-curve of E-glass/epoxy laminated composites. Compos Struct 2017; 171: 19-31.
[24] H Silva, JAM Ferreira, C Capela, MOW Richardson. Mixed Mode interlayer fracture of glass fiber/nano-enhanced epoxy composites. Compos A Appl Sci Manuf 2014; 64: 211-22.
[25] A Laksimi, A Ahmed Benyahia, ML Benzeggagh, XL Gong. Initiation and bifurcation mechanisms of cracks in multi-directional laminates. Compos Sci Technol 2000; 60: 597-604.
[26] TA Sebaey, N Blanco, J Costa, CS Lopes. Characterization of crack propagation in mode I delamination of multidirectional CFRP laminates. Compos Sci Technol 2012; 72: 1251-6.
[27] Y Gong, B Zhang, SR Hallett. Delamination migration in multidirectional composite laminates under mode I quasi-static and fatigue loading. Compos Struct 2018; 189: 160-76.
[28] Y Gong, B Zhang, S Mukhopadhyay, SR Hallett. Experimental study on delamination migration

in multidirectional laminates under mode II static and fatigue loading, with comparison to mode I. Compos Struct 2018; 201: 683-98.
[29] M Kenane, Z Azari, S Benmedakhene, ML Benzeggagh. Experimental development of fatigue delamination threshold criterion. Compos Part B Eng 2011; 42: 367-75.
[30] ASTM Standard D5528-13, Standard Test Method for Mode I Interlaminar Fracture Toughness of Unidirectional Fiber-Reinforced Polymer Matrix Composites. ASTM International, 2013.
[31] ASTM Standard D6671/D6671M-13e1, Standard Test Method for Mixed Mode I-Mode II Interlaminar Fracture Toughness of Unidirectional Fiber Reinforced Polymer Matrix Composites. ASTM International, 2013.
[32] F Brandt. New load introduction concept for improved and simplified delamination beam testing. Exp Techniques 1998; 22: 17-20.
[33] J Jumel, MK Budzik, N Ben Salem, M Shanahan. Instrumented End Notched Flexure-crack propagation and process zone monitoring Part I: Modelling and analysis. Int J Solids Struct 2012.
[34] XJ Gong, A Hurez, G Verchery. On the determination of delamination toughness by using multidirectional DCB specimens. Polym Test 2010; 29: 658-66.
[35] M Heidari-Rarani, MM Shokrieh, PP Camanho. Finite element modeling of mode I delamination growth in laminated DCB specimens with R-curve effects. Compos Part B Eng 2013; 45: 897-903.
[36] X Gong, M Benzeggagh. Mixed Mode Interlaminar Fracture Toughness of Unidirectional Glass/Epoxy Composite. Composite Materials: Fatigue and Fracture: Fifth Volume. West Conshohocken 1995; 100-23.
[37] RM Marat-Mendes, MM Freitas. Failure criteria for mixed mode delamination in glass fibre epoxy composites. Compos Struct 2010; 92: 2292-8.
[38] M Fakoor, NM Khansari. General mixed mode I/II failure criterion for composite materials based on matrix fracture properties. Theor Appl Fract Mec 2018; 96: 428-42.

Figure Captions

Fig. 1. A sketch showing the occurrence of the fibre bridging in the +22.5°/-22.5° interface.

Fig. 2. Sketches of the experimental set-ups for the DCB, MMB and ENF tests.

Fig. 3. Typical load-displacement curves for the DCB/MMB/ENF specimens with the (a) 0°/0° interface and (b) +22.5°/-22.5° interface.

Fig. 4. Fracture toughness versus the delamination growth length for the 0°/0° interface.

Fig. 5. Fracture toughness versus the delamination growth length for the +22.5°/-22.5° interface.

Fig. 6. Fracture toughness G_{I} versus G_{II} for the (a) 0°/0° and (b) +22.5°/-22.5° interfaces. Note: a constant mode II fracture toughness is used for each interface.

Fig. 7. Initiation and steady-state propagation failure loci for the (a) 0°/0° and (b) +22.5°/-22.5° interfaces.

Fig. 8. Comparison of the experiment MMB *R*-curves and the predicted ones by Eq. (13), (a) 0°/0° interface and (b) +22.5°/-22.5° interface.

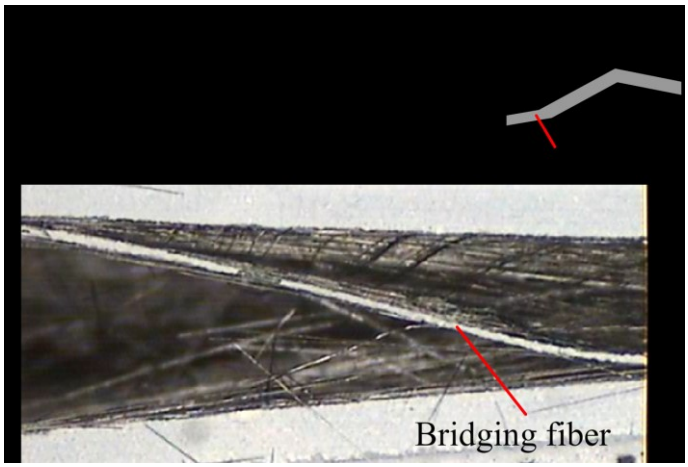

Fig. 1. A sketch showing the occurrence of the fibre bridging in the +22.5°/-22.5° interface.

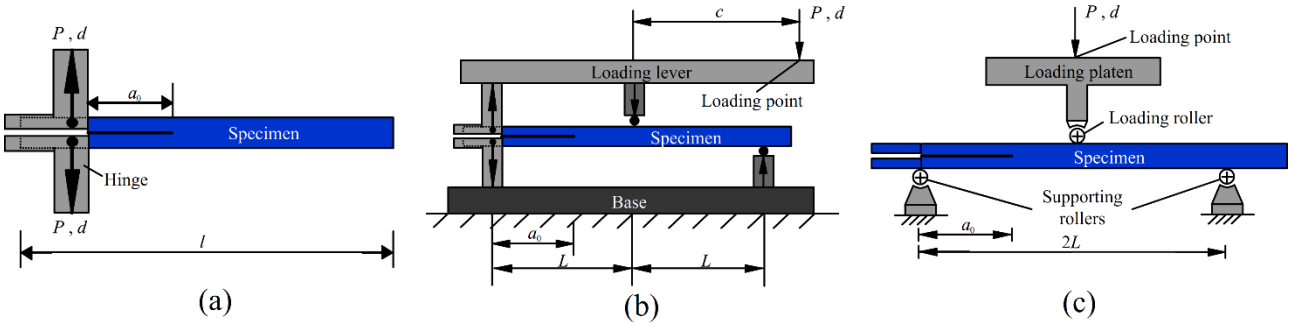

Fig. 2. Sketches of the experimental set-ups for the DCB, MMB and ENF tests.

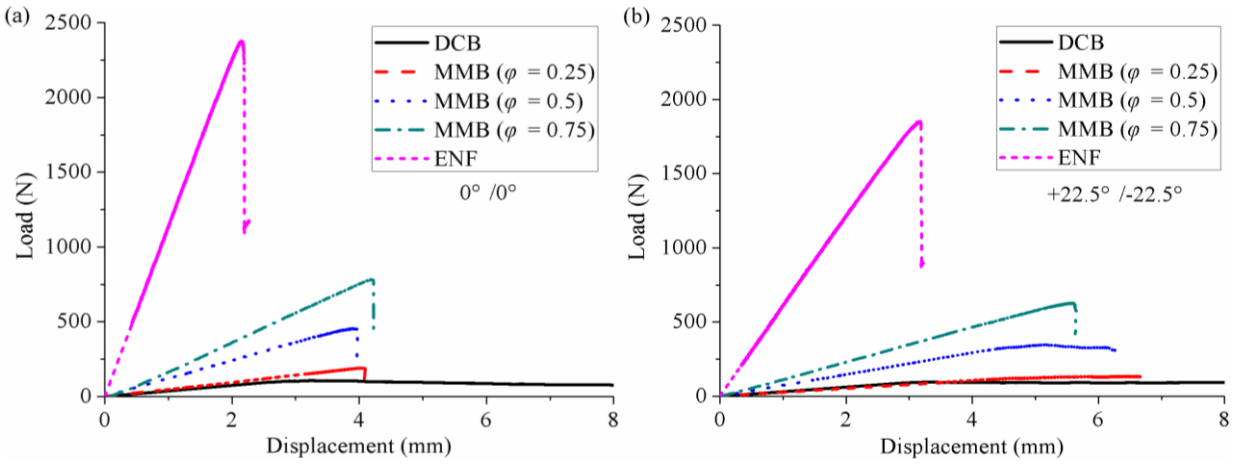

Fig. 3. Typical load-displacement curves for the DCB/MMB/ENF specimens with the (a) 0°/0° interface and (b) +22.5°/-22.5° interface.

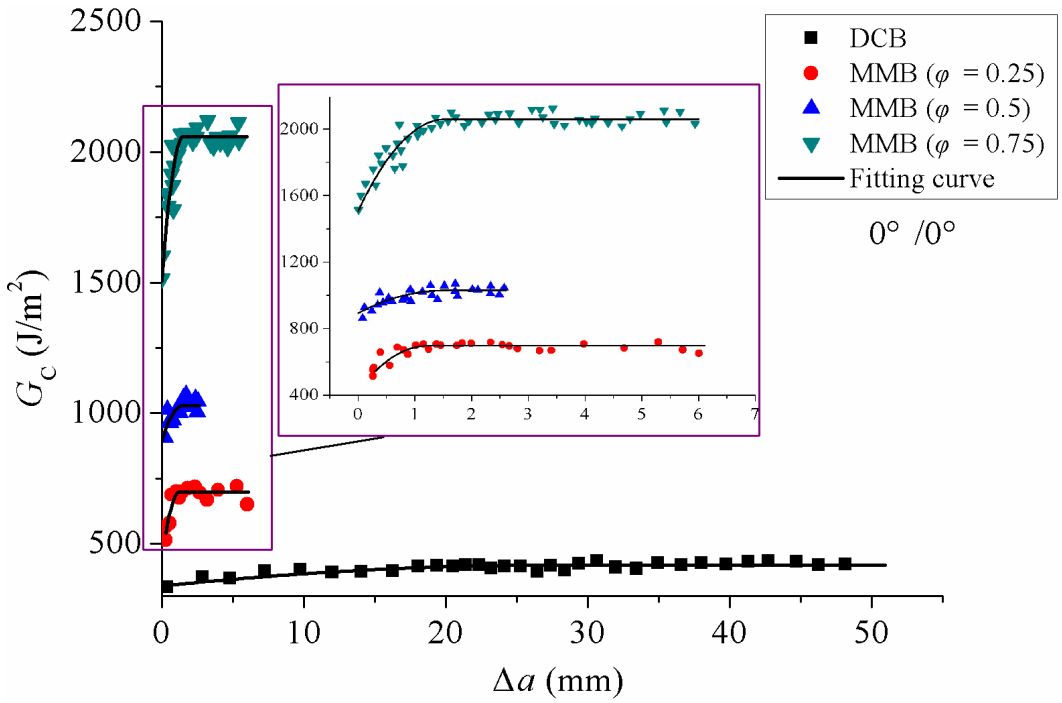

Fig. 4. Fracture toughness versus the delamination growth length for the 0°/0° interface.

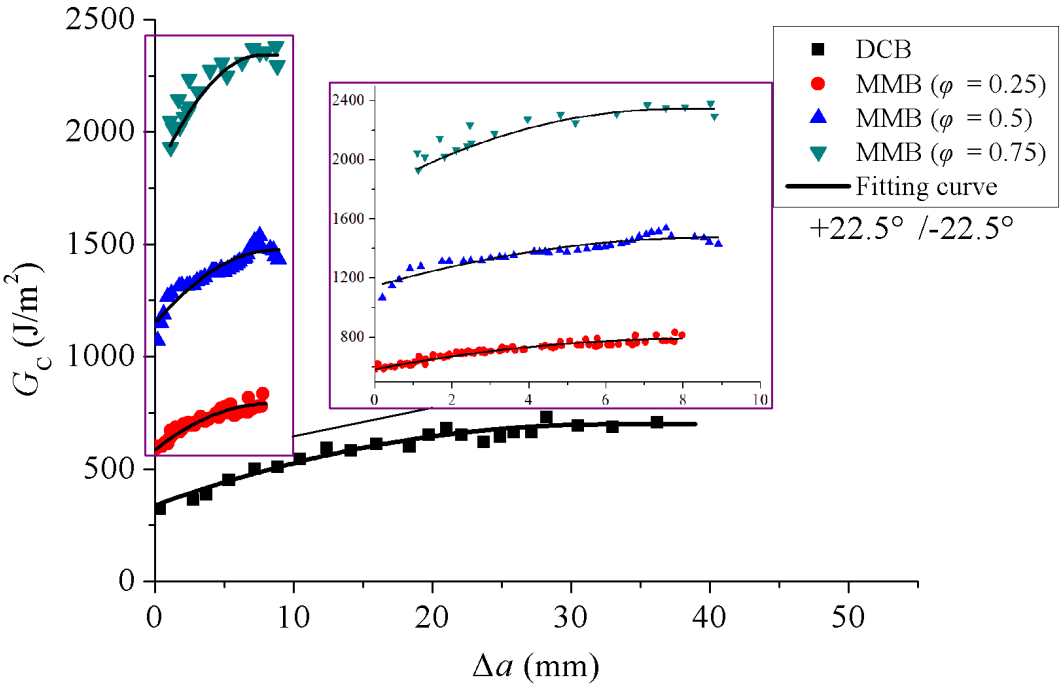

Fig. 5. Fracture toughness versus the delamination growth length for the +22.5°/-22.5° interface.

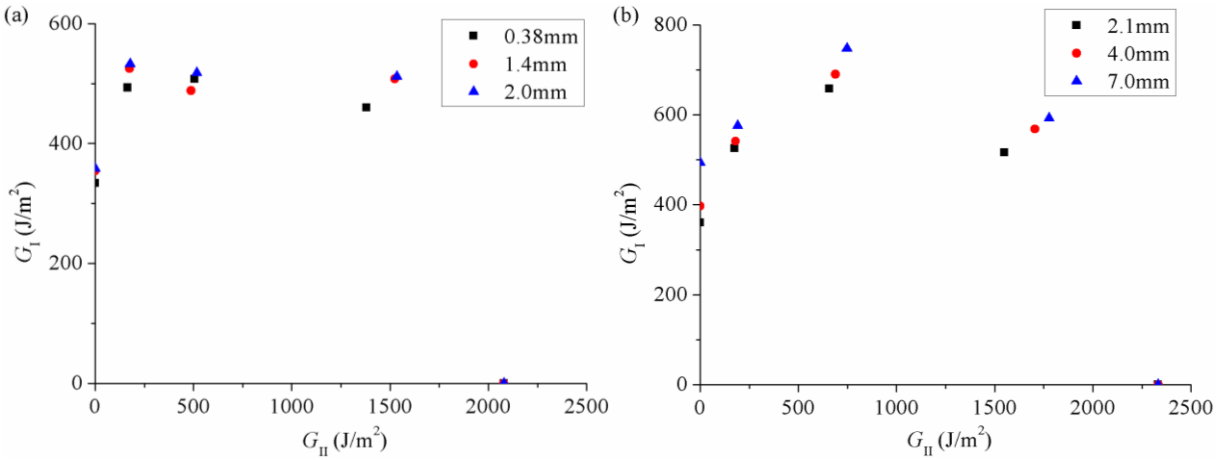

Fig. 6. Fracture toughness G_I versus G_{II} for the (a) 0°/0° and (b) +22.5°/-22.5° interfaces. Note: a constant mode II fracture toughness is used for each interface.

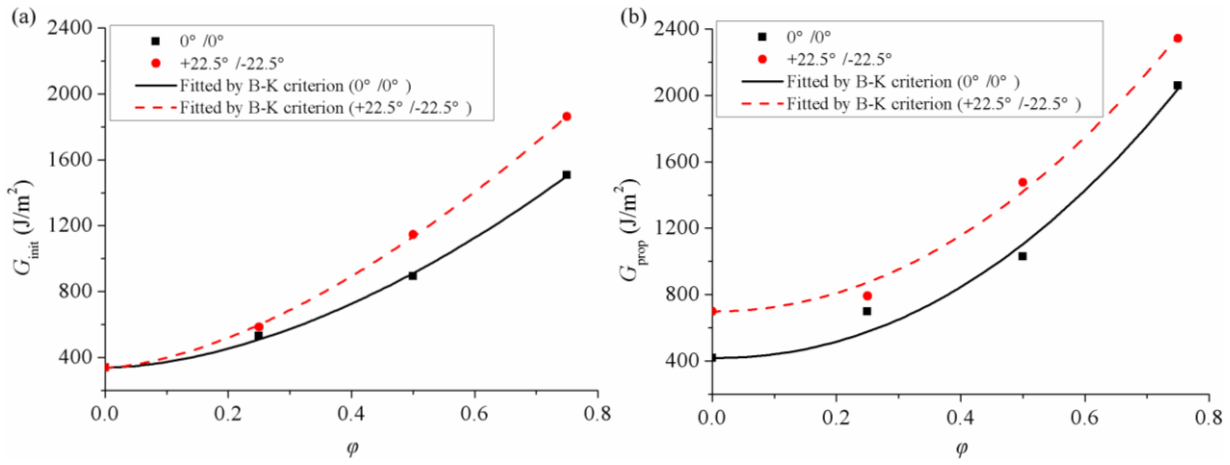

Fig. 7. Initiation and steady-state propagation failure loci for the (a) 0°/0° and (b) +22.5°/-22.5° interfaces.

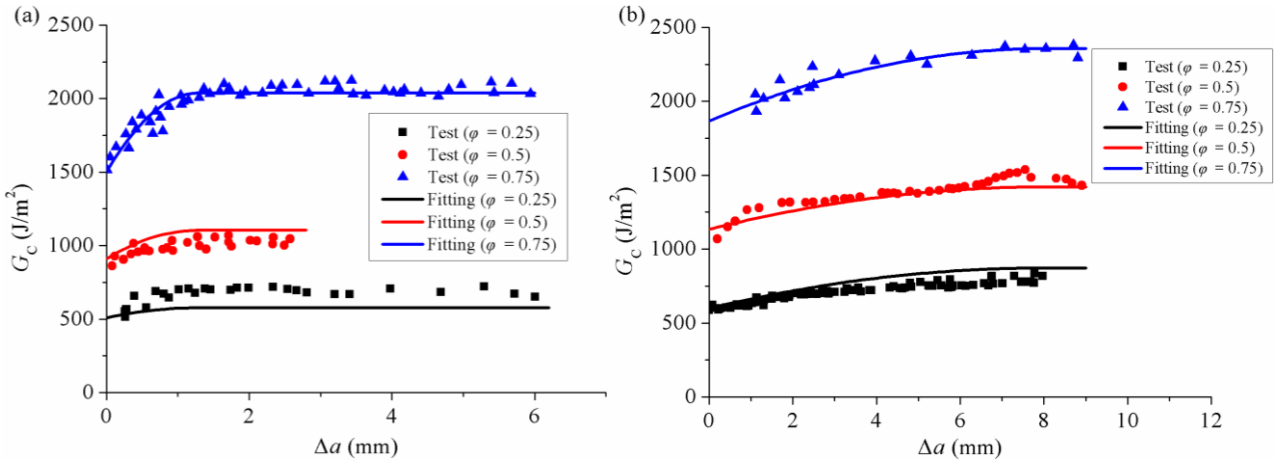

Fig. 8. Comparison of the experiment MMB *R*-curves and the predicted ones by Eq. (13), (a) 0°/0° interface and (b) +22.5°/-22.5° interface.

Table Captions

Table 1 Values of the lever length c for the MMB tests (Unit: mm).

Table 2 Detailed values of l_{bz}, G_{Init} and G_{Prop} for each interface and φ-ratio.

Table 3 Comparison of the experimental and predicted values of the mode II fracture toughness.

Table 1 Values of the lever length c for the MMB tests (Unit: mm).

Interface	φ-ratio		
	0.25	0.5	0.75
0°/0°	81.6	45.6	31.7
22.5°/-22.5°	81.0	44.7	31.5

Table 2 Detailed values of l_{bz}, G_{Init} and G_{Prop} for each interface and φ-ratio.

Interface	φ-ratio	l_{bz} (mm)	G_{Init} (J/m^2)	G_{Prop} (J/m^2)	G_{Prop}/G_{Init}
0°/0°	0	28.4	338.9	418.9	1.24
	0.25	1.2	531.5	697.6	1.31
	0.5	1.2	893.5	1029.2	1.15
	0.75	1.5	1507.5	2058.7	1.37
	1	/	2078.8	/	/
+22.5°/-22.5°	0	32.6	339.0	699.0	2.06
	0.25	8.3	584.8	791.4	1.35
	0.5	8.8	1160.5	1475.0	1.27
	0.75	7.2	1997.1	2342.9	1.17
	1	/	2333.3	/	/

Table 3 Comparison of the experimental and predicted values of the mode II fracture toughness.

Interface	Initial value (J/m^2)		Relative error	Steady-state value (J/m^2)		Relative error
	Test	Predicted	(%)	Test	Predicted	(%)
0°/0°	2078.8	2262.2	8.8	/	3400.4	/
22.5°/-22.5°	2535.3	2765.8	9.1	/	3690.1	/